Journal of Genomic Medicine and Pharmacogenomics
JGMP, 4(1): 351-363
www.scitcentral.com

ISSN: 2464-4670

Original Research Article: Open Access

Efficient Removal of Drugs from Aqueous System with Graphene Based Nanocomposite Derivatives with Magnetic Chitosan

Farid Abu Shammala[1*] and Barry Chiswell[2]

[*1]*Department of Pharmacy, University of Palestine, El-Zahra City, Gaza, Palestine*

[2]*National Research Centre for Environmental Toxocology, University of Queensland, Brisbane, Australia.*

Received December 19, 2018; Accepted January 01, 2019; Published November 21, 2019

ABSTRACT

In the current study, a green approach to the synthesis and functionalization of GO–Chm nano composite by the reaction of graphite oxide (GO) with magnetic chitosan (Chm) was investigated. GO–Chm nanocomposite was tested as photocatalysts for adsorption and removal of four drugs: tetracycline, Ciprofloxacin, lincomycin and ranitidine from aqueous solution. The synthesis mechanism of GO–Chm nanocomposite was studied and characterized with Scanning electron microscopy (SEM), Fourier transform infrared spectroscopy (FTIR), X-ray photoelectron spectroscopy (XPS), Raman spectroscopy, Atomic force microscopy (AFM) image analysis, UV-Vis spectra, X-ray diffraction patterns, thermogravimetric analysis (TGA) and Differential scanning calorimetry (DSC). Dielectric and Conductivity Properties of GO–Chm nanocomposite was measured. Results confirms reduction of GO to graphene by magnetic chitosan. Adsorption process of drugs onto GO–Chm is inner sphere type, indicating that the surface complexation of drug with GO–Chm is very strong. The adsorption capacity of TC to GO–Chm nanocomposite was the highest (approx. 575.5 mg/g). The calculated maximum adsorption capacities of tetracycline, Ciprofloxacin, lincomycin and ranitidine from aqueous solution under UV light were 575.5, 168.2, 75.8 and 218.2 mg/g, respectively). The effect of pH on accumulation and degradation of drugs revealed that the acidic conditions (pH3) are favorable. Kinetic experiments showed that the adsorption phenomenon follow a pseudo-second-order equations, the equilibrium data were fitted to the Langmuir, Freundlich (L–F) models.

Keywords: Graphene oxide, Magnetic chitosan, Nanocomposites, Drug, Tetracycline, Ciprofloxacin, Lincomycin and ranitidine, Photodegradation, Photocatalysis

INTRODUCTION

Frequently, pharmaceuticals and personal care products (PPCPs) have been detected in our environment and in our environment and they have attracted scrutiny as a new type of wastewater pollutant that threatens the human health an biosphere [1,2]. PPCPs have also been used as growth promoters for livestock, bees, aquatic products and other aquaculture industries [3,4]. The average total annual use of antibiotics is approximately 200,000 tons [4,5]. For a variety of well-known drugs and antibiotics, tetracycline, ciprofloxacin, lincomycin and ranitidine attracts more attention because of their wide use and large production [6-8], among which TCs are some of the most frequently detected antibiotics in biosphere wastewater [9]. Indeed for most antibiotics their intermediate products known to be toxic, mutagenic and emerging pollutants due to their continuous input and persistence in the aquatic ecosystem. Complete removal of these toxic antibiotics intermediate from industrial waste is becoming more important due to their harmful effect on living organism. Meanwhile, the abuse of antibiotics also results in huge quantities of antibiotic found in wastewater, by which bacterial resistance was introduced to natural ecosystems [10,11]. Recent researches have showed that 68 different antibiotics were detected in some surface water [12], making the treatment of antibiotic wastewater becomes a global concern in public health and environment. Different type of methods have been utilized for the removal of antibiotic from wastewater, such as chemical oxidation [4], biodegradation [13],

Corresponding author: Farid Abu Shammala, Adjunct Professor, Faculty of Pharmacy, University of Palestine, Gaza, Palestine, E-mail: drfaridshammala@hotmail.com

Citation: Shammala FA & Chiswell B. (2019) Efficient Removal of Drugs from Aqueous System with Graphene Based Nanocomposite Derivatives with Magnetic Chitosan. J Genomic Med Pharmacogenomics, 4(1): 351-363.

adsorption [14], liquid extraction [15] and membrane techniques [16,17]. Among these methods, the adsorption process is regarded as a promising method for the removal of various organic compounds because of its simple design, low-cost, high efficiency, and less production of toxic intermediates. So, it is of great importance to study and develop a new and efficient method for accumulation and removal of these drugs using GO–Chm nanocomposite.

Graphene and graphine oxide are the most basic form of carbon, it is composed of sp^2 bonded carbon atoms arranged in a hexagonal arrangement in a 2D plane [16]. The lattice of graphene consists of two interleaved triangular shaped carbon sublattices. The sublattices overlap in such a way that carbon atom from one sublattice is at the centroid of the other sublattice [17-19]. Graphene has been utilized in many engineering and industrial applications to create composite materials with superior qualities such as functional fluids, lubricants and high temperature gaskets. In these applications, one-carbon-atom thick graphene can be a very promising reinforcing agent [20-22] and provide exceptional electrical and thermal transport properties compared to other nanomaterials such as layered silicates or carbon nanotubes (CNTs) [23-25]. Indeed, graphene-based polymer nanocomposites exhibit superior promising properties. For example, graphene-based polymer composites show better thermal, mechanical and electrical properties than the normal polymer [26,27]. It has been shown that the mechanical and electrical properties of graphene-based polymer composites are much better in comparison to clay or other carbon filler-based polymer composites [28-32]. One of the main applications of graphene sheets is use as reinforcement agents for the preparation of nanocomposites with different types of polymers. Other than mechanical properties, electrical and thermal properties of the polymeric matrix can also be enhanced. It is a fact that the graphene-based nanocomposites present improved properties compared to the original raw form of graphene. Graphene nanocomposites with polysaccharides such as chitosan have many diverse new applications. Polysaccharide exist both as linear or branched polymers, since their repeating monosaccharide units are connected via O-glycosidic bonds [33]. Their properties, including gelation, water solubility and other surface properties depend on the type of monosaccharide composition. Advantages such as abundance in nature, biocompatibility, biodegradability, easy functionalization and relatively easy isolation from their natural sources have led to their study and use in several applications, especially in the field of drug delivery and biomaterials [34]. Another application of graphene derivatives with polysaccharide is the use in accumulation and removal of various types of pollutants from wastewater effluents [35]. Graphene nanocomposites with chitosan have been used for the removal of dyes [36,37], heavy metal ions [38] and pharmaceutical compounds [39] from aqueous solutions. Despite the intriguing properties of polysaccharides, their poor mechanical properties limit their applications. Nanofillers such as graphene are known to improve the properties of raw polymers, not only the mechanical but also the thermal and electrical properties [40,41]. Moreover, the effects of the incorporation of graphene and graphene oxide together in raw polymers have been extensively studied, mostly synthetic polymers reinforced by graphene and graphene oxide find several improvement in properties such as mechanical strength, thermal stability, gas barrier properties, electrical and thermal conductivity, etc. [42-49].

The final properties of nanocomposites depend on various factors; the most important is the interfacial bonding between the filler and the matrix. Poor adhesion can lead to aggregates of the nanofillers or gaps between the surface of the composites components, acting as stress concentration points and therefore causing premature failure of the materials. Besides, the compatibility between nanofiller and matrix, the geometrical and the aspect ratio of the fillers play a similarly important role. Graphene possesses a high surface area, high aspect ratio, and high strength which are reasons for the enhanced performance of its nanocomposites. Large graphene or GO flakes with high surface areas have proved to be more efficient reinforcing agents than similar structures with smaller aspect ratio.

In this review article, the recent advances of the last decade in synthesis and applications of graphite oxide (GO) with magnetic chitosan (Chm) was investigated to prepare a nanocomposite material (GO–Chm). These will be compared regarding their mechanical properties as well as their various applications. The effect of GO on the properties of magnetic chitosan films has been studied using solution mixing. Strong interactions between the functional groups of the two components, confirmed by FTIR spectra, led to a series of improved properties, including mechanical strength in both wet and dry state, storage modulus, and thermal stability. The fabricated magnetic chitosan (Chm) nanocomposites with GO with large area have better mechanical and thermal properties to the nanocomposites,

GO–Chm nanocomposites were synthesized by adding magnetic Fe_3O_4 particles in GO–Ch, followed by the dispersion of GO in the magnetic CS solution via ultrasonication. The graphine-based nanocomposite derivatives with magnetic chitosan were applied in absorbing antibiotics, such as tetracycline, Ciprofloxacin, lincomycin and ranitidine from aqueous solution under UV light. The results of our studies showed that drugs strongly loads on the GO–Chm nanocomposite derivative surface via π–π interaction and cation–π bonding. The adsorption behavior of the prepared composite was elucidated with a series of experiments. The tests of the effects of pH revealed that the adsorption mechanism dominated between drug molecules and the GO–Chm matrix and showed that acidic conditions were the optimum for the adsorption process (pH

3). After 5 h, under visible light an appreciable photolytic degradation of tetracycline and ranitidine was observed while the degradation of lincomycin and ciprofloxacin was noticeably lower. The presence of UV light the photocatalysts degradation of all drug tested greatly enhanced compared to the drugs degradation rates observed during the visible light experiments. The Langmuir-Hinshelwood kinetic model adequately describes the experimental results and both the pseudo-first order kinetic constants of the reactions and the adsorption constants were calculated. GO–Chm was more active than GO alone for the photodegradation of tetracycline, ciprofloxacin and ranitidine, whereas both photocatalysts showed similar performances for lincomycin. In the presence of GO–Chm, under UV illumination tetracycline was almost completely degraded, but the reduction of 90% was observed in the case of ciprofloxacin and ranitidine. Graphene magnetic chitosan nanocomposites (GO–Chm) offer a green alternative to synthetic polymers in the preparation of soft nanomaterials, results indicated that a significant fraction of the amines of the chitosan (i) were inserted between the GO layers and (ii) reacted with carboxyl and epoxy groups of GO, leading to its reduction and hence the destruction of the layered structure.

EXPERIMENTAL

Materials

Graphene (GE) and magnetic chitosan (Chm) used in our studies were purchased from Sigma-Aldrich. Analytical grade chemical reagents like potassium persulfate ($K_2S_2O_8$) and hydrochloric, sulfuric and nitric acid used in our experiments were obtained from Sigma Chemicals. GE was reacted with mixture of two acids H_2SO_4 and HNO_3 acids with 3:1 ratio and later sonicated for 60 min using an ultrasonic sonicator to form carboxylic acid functionalized GO (GO-COOH). The carboxylic acid group was converted to formyl chloride by reaction with thionyl chloride for 24 h at 80°C. Then the reaction was stopped and the mixture was cooled before centrifuging and washing to remove excess reactants. The sample was then dried overnight at a temperature of 90°C and 30 Hg pressure.

Synthesis of GO-magnetic chitosan

The formyl chloride of GO (GO-COCl) (400 mg) was then reacted with chitosan (2 g) in 100 mL 2% acetic acid at 75°C for 24 h while magnetic stirring. In order to remove the unreacted chitosan, the product was washed three times with 3% acetic acid after the reaction was stopped.

Synthesis of GO-chitosan grafted derivative

GE-chitosan complex (0.1 g) was then reacted with $K_2S_2O_8$ (0.02 g) in 2% acetic acid solution at 80°C for 4 h to form the nanocomposite product GE-Chm. The final product was prepared by centrifuging at 20,000 rpm and washing the sample three times with deionized water before drying at 90°C. The GO-Chm was produced using a chemical co-precipitation method with iron oxide. Iron (III) oxide (Fe_2O_3) nanoparticles (5.8 g) were produced by dissolving ferrous ammonium sulfate in (10.7 g) of ammonium ferric sulfate in 100 mL deionized water to form a mixed iron salt solution under oxygen-free conditions. Chemical precipitation was achieved by adding a 75 mL ammonium hydroxide (NH4OH) solution (30.0%) drop-wise for a period of 30 min at 30°C. After the addition of ammonium hydroxide a black precipitates appeared immediately and the precipitated particles exhibited a strong magnetic response. Next, 2 g dry GO-Chm was dispersed in 200 mL ultrapure water using ultra-sonication to form a stable suspension. Finally, the GO-Chm solid was collected using a magnet and was washed with deionized water and anhydrous ethanol three times each and dried at 90°C for 24 h in a vacuum oven. Our results show a strong affinity between water and the different groups attached to graphene sheets. Indeed, dispersions with water show the darkest color for the longer time, pure graphite can be dispersed only partially and a high number of particles remain adhered to the container walls. However, after sonication and 12 h kept at rest the carboxyl and hydroxyl groups in GO and Chm allows the formation of a stable dispersion in water. For chitosan-grafted samples, the hydrophilic nature of chitosan facilitates the interactions between water and amine, as well as carbonyl and hydroxyl groups. However, it is important to mention that dispersion related to graphene oxide grafted with chitosan obtained at the temperature range of 60°C is better after 24 h than the other samples of grafted graphene oxide. On the other hand, dispersion of graphene oxide in hexane is poor, the absence of suitable chemical groups to interact and the non-polar nature of the solvent cause the nanosheets to precipitate rapidly, regardless of moieties attached to GO-Chm and grafted samples.

Adsorption procedure

The prepared GO–Chm nancomposites with superparamagnetism were then used to test adsorption ability for drug. The prepared GO–Chm nancomposites with superparamagnetism can be separated by a magnet after the adsorption process. All sorption experiments were carried out in in triplicate and the average values were adopted. The maximum deviation for the duplicates was usually less than 5%; 5 mg absorbents and 50 ml drug solution were put in 50 ml glass bottles and processed within an incubator shaker at a frequency of 100 rpm. The initial concentration of drug is 0-50 mg/L. Meanwhile, the blank experiments without absorbents were also conducted to confirm that the decrease of drug concentration was because of absorbents instead of any other factors. After the adsorption process, the drug concentration was measured by the UV spectrophotometer at the peak of λ_{max}=356 nm was used for Tetracycline, λ_{max}=272 for Ciprofloxacin, λ_{max}=213.5 for ranitidine and λ_{max}=196 for lincomycin. A calibration curve between absorbance and concentration of drug (0 - 20 mg/L) was constructed according to the Beer-Lambert's Law. For

solutions with concentration higher than 20 mg/L, the solutions were first diluted with deionized water. Kinetic studies were performed at a constant temperature of 25°C and 100 rpm with 50 mg/L initial concentration of drug solutions with different adsorption time. The solid-liquid ratio experiments were conducted in 100 mg/L drug solutions with varying solid-liquid ratio from 1:10 to 1:2. The effect of drug solution pH on the accumulation and removal of drug was studied in the range of 3-10 with 100 mg/L initial concentrations of drug solutions. The initial pH values of all the solutions were adjusted using 0.1 mol/L HCl or 0.1 mol/L NaOH solutions with desired concentrations. The ionic strength experiments were conducted in 100 mg/L drug solutions with varying ionic strength range from 0 to 2. 5 mmol/L.

RESULTS AND DISCUSSION

Characterization using SEM image

GO–Chm nanocomposite surface morphology was investigated by a scanning electron microscope. In order to examine the influence of the graphene chemical functionalities on the morphology of graphene-based composites, GO and GO–Chm were blended with the polymer matrix. The SEM images in **Figure 1b** show the cross sections of composites containing 3 wt% of Chm in GO sheet. The images shows GO is dispersed in the composite due to the formation of agglomerates at length scales of tens of microns. The typical SEM images of GO presents a wrinkled sheet-like structure, as shown in **Figure 1a**. **Figures 1b and 1c** show a better distribution of GO particles homogeneously covered by the Chm polymer. The copolymer-modified graphene composite can be homogeneously integrated within hydrophilic Chm matrix. The presence of ionic moieties such as alkyl amino and carboxylates in the polymer backbone can result in enhanced interfacial interactions between the filler and the matrix. Upon functionalization with GO–Chm, the SEM image of GO–Chm **(Figure 1b)** has a much rougher surface and greater thickness, which demonstrates that many polymer chains have been assembled on the surface of the GO sheets. TEM image of GO **(Figure 1c)** shows a transparent sheet with the presence of folded regions at the edges. TEM image of the GO–Chm **(Figure 1d)** presents a thick and rough sheet-like material, demonstrating that CS-PHGC composites have been assembled on the GO sheets.

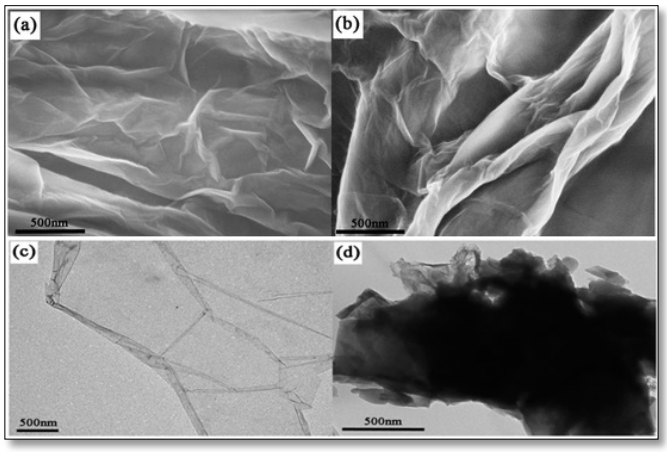

Figure 1. SEM images of (a) GO and (b) GO–Chm; TEM images of (c) GO and (d) GO–Chm.

FTIR spectra

The mechanism of chemical reaction due to grafting of magnetic chitosan onto graphene oxide was studied using FTIR. The interactions of different functional groups during grafting were observed in all graphene samples through FTIR analysis is shown in **Figure 2**. The peaks of GO appeared at 1720 cm^{-1} (C=O in carboxyl group), 1620 cm^{-1} (C=C in the aromatic ring), 1380 cm^{-1} (C–OH functional group) and 1100 cm^{-1} (is for vibration of an epoxide group). For the GO–Chm nanocomposite, the absorption peak for C=O in the carboxyl group has disappeared and the peaks of C–OH and epoxide group are shifted to 1382 cm^{-1} and 1100 cm^{-1}, respectively, which is apparently may be due to the encapsulates of the groups of Fe_3O_4 on the surface of GO–Ch. The peak appeared at 540 cm^{-1} corresponds to the stretching vibration of the Fe–O bond. The pure graphite FTIR is observed in **Figure 2a**, whereas GO–Ch FTIR and GO–Chm FTIR spectra (**Figures 2b and 2c**, respectively) show several distinctive signals such as: 1730 cm^{-1}, ν(C=O) of carboxyl groups; 1621 cm^{-1}, ν(C=C); and 1064 cm^{-1}, ν(C–O). All these signals and moieties give evidence of the presence of oxygen-containing groups, caused by the chemical reaction. For the GO–Chm nanocomposite FTIR new signals were observed because of interactions between carbonyl and hydroxyl groups from GO and chitosan moieties: amino, hydroxyl and RNHCOCH3, this last from remaining acetylated parts of chitosan. At 1534 cm−1 a new band is observed in GO–Chm spectra **(Figure 2D)**. It can be assigned to the combination of the ν(C–N) with the δ(CHN) (amide II), which is apparently corresponds to amides or carbamate esters formed during the grafting reaction. The signal at 1155 cm^{-1} is attributed to νa(C–O–C) and the band at 900 cm^{-1} corresponds also to C–O–C, in both cases related to the glycosidic linkage. These signals, typical in chitosan, were absent in GO spectra, but they appear with a clear shift (889 cm^{-1}) in GO–Chm spectra. This indicates that C–O–C bond vibrations are also modified due to grafting treatment; when C–O– bonds of chitosan interact

with GO to form GO–Chm nanocomposite hybrids. Thus, not only amine groups can take part in grafting, also the OH, of the chitosan structure can play an important role during chemical interaction.

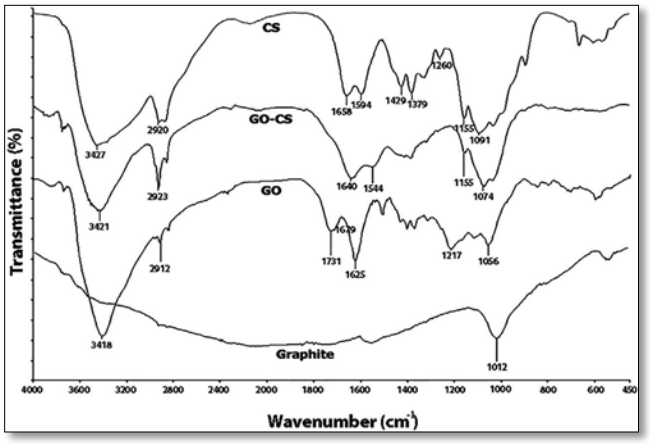

Figure 2. Fourier transforms infrared spectroscopy (FTIR) spectra of: graphite; graphine oxide (GO); chitosan (CS); (D) GO–CS nanocomposite.

X-ray photoelectron spectroscopy (XPS) measurements

XPS was investigated to further explore the mechanism of interactions between GO and Chm. The survey of GO **(Figure 3a)** shows that no detectable amount of N1s, for the strongest XPS band of N-is usually found between 400 and 407 eV depending on the chemical environment. **Figure 3b** shows the N1s XPS spectra of chitosan, with three different peaks centered at 399.0, 400.5 and 401.6 eV. These peaks correspond to C-NH2, C-NHC=O and C-N+, respectively. For GO–Chm nancomposite the survey (shown in **Figure 3c**) shows the presence of N1s originating from chitosan. The N1s spectrum of GO-chitosan can be resolved into three peak components with binding energies at 399.4, 400.7 and 401.7 eV, attributed to the amine, amide and the protonated amine species, respectively. Compared with chitosan, the relative increase in amide peak and decrease in protonated amine in GO–Chm nancomposite provides conclusive evidence for the formation of new covalent functionalization between the carboxylic acid on the surface of GO and N groups of magnetic chitosan. These results are consistent with the results observed in the FTIR analysis.

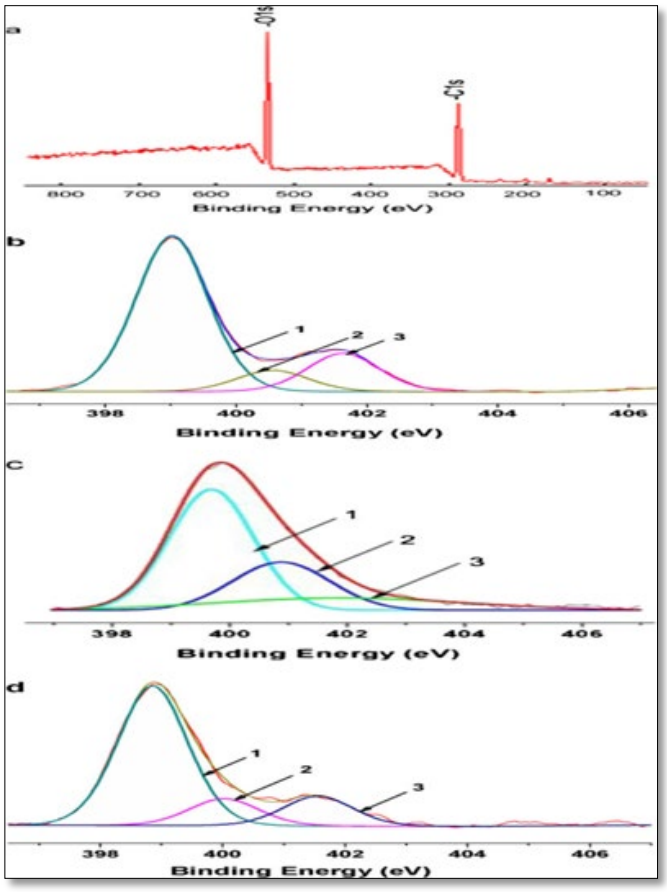

Figure 3. X-ray photoelectron spectroscopy of N1s core-level spectra of (a) GO, (b) chitosan, (c) GO–chitosan nancomposite and (d) GO–Chm nancomposite (The peaks 1, 2 and 3 correspond to $C\text{-}NH_2$, C-NH-C=O, $C\text{-}N^+$, respectively).

Raman spectra

Figure 4 shows Raman spectra of GO and GO–Chm nanocomposite, it shows distinctive signals for each one of them. The strong band shown close to 1579 cm^{-1} (G band), a line around 1351 cm^{-1} (D band) and 2D band in the region around 2700 cm^{-1}. The observed tangential G mode corresponds to the first-order scattering of the E2g mode in-phase vibration of the GO lattice. Indeed, the D band is due to the out-of-plane breathing mode of the sp^2 atoms, it reveals the presence of certain defects, whereas 2D is the second order of this vibrational mode. In the spectrum of pure graphite it was observed that the D and G modes are weak. However, after interaction between Chm and exfoliation of GO nancomposite (GO–Chm) both modes become wider and increase in their intensity. The obvious well defined peak of the 2D band in the pure GO spectrum undergoes certain changes after interaction with Chm. It goes out of shape and even disappears in GO–Chm nanocomposite. These variations in Raman spectrum confirm the modification and layer separation of the carbon

structure. The spectrum shows the formation of some sort of crystallinity, doping and layer ordering of the sp^2 sites of GO–Chm nanocomposite. Indeed, these interactions affect positions, intensities and widths of the D and G bands. In the same sense, the intensity and breadth of the 2D band in graphene depends on the number of carbon layers. The 2D band is a second-order process related to a phonon near the K point in reduced graphene, activated by double resonance processes, is responsible for its dispersive nature and causes a strong dependence on perturbation of the electronic structure of reduced graphene during interaction with magnetic chitosan. Therefore, the 2D band is very predisposed to characterize specific sp2 nanocarbons in the GO–Chm nanocomposite. And D and G bands show a shift, broadening and increasing as a result of the covalent attachment of the magnetic chitosan to the graphene sheet. Band broadening is evidently related to the changes produced in the graphene oxide layers by the grafted chitosan.

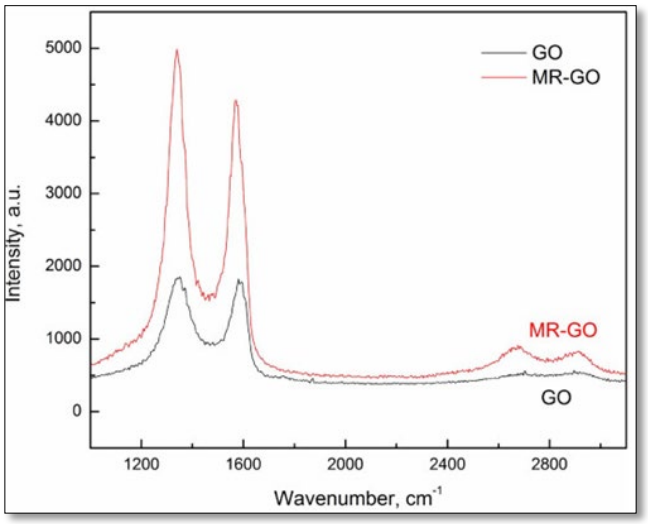

Figure 4. Raman spectra of GO and chitosan-grafted graphene oxide GO–Chm.

Atomic force microscopy (AFM) image

Figure 5a shows an atomic force microscopy (AFM) image of GO–Chm nancomposite sheet, where it is possible to observe in this image an irregular structure with different thicknesses that reach up to 296 nm (topography graph, **Figure 5c**). The AFM shows that the grafted chitosan after reaction only covers a few nanometers when it is coupled to the graphene sheet.

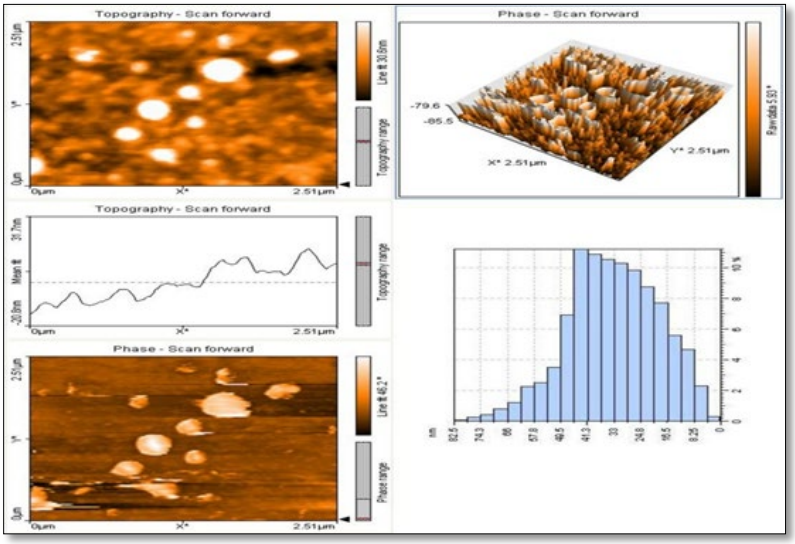

Figure 5. Atomic force microscopy (AFM) image of GO–Chm nancomposite sheet and its topography and size distribution a) two-dimensional, b) three-dimensional c) size distribution.

AFM images in **Figures 4d and 5c** shows irregular surface of graphene oxide sheets, with notched shapes and roughness, the average height was measured at 0.57 nm. AFM images of GO–Chm nancomposite sheets shown in **Figure 5**, where it is possible to observe variations in height from 3 to 6 nm, this increment in thickness is due to magnetic chitosan grafting covering both sides of the GO sheet. **Figure 5c** shows a dense areas corresponding to a height of 6 nm, these are attributed to bundles of magnetic chitosan chains grafted onto GO sheets.

UV-Vis spectra

The UV-Vis spectra of GO–Chm nancomposite **(Figure 6b)**, after samples dispersed in water with sonication and 24 h kept to rest shows two absorption peaks one at 234 nm and another at 304 nm. The Chm peaks are seen at 240 nm and 280 nm. After attachment with Chm, the peaks of GO have shown a bathochromic shift. This shift in absorption maxima might be attributed to the formation of particles in the nano scale. This also confirm the strong covalent interaction between GO and Chm where the active ester group of GO might have reacted with the amine groups on Chm, forming an amide bond between GO and Chm. Optical analysis shows the band gap energy of GO to be 1.02 eV and that of the nanocomposite to be 1.08 eV. Since these values are within the range of semiconductor indicating that the conductivity of the constituents are retained in the composites thus enabling their application in the field of optoelectronics. The peak related to the π–π* transitions near to 230 nm and the shoulder at 300 nm due to n–π* transition are clear and more intensive in GO and Chm spectra, giving evidence that better dispersion is reached even maintaining at rest for 24 h. Also, it is evident than GO–Chm is the grafted sample that maintains absorption due to better dispersion than the other two GO–Chm grafted samples.

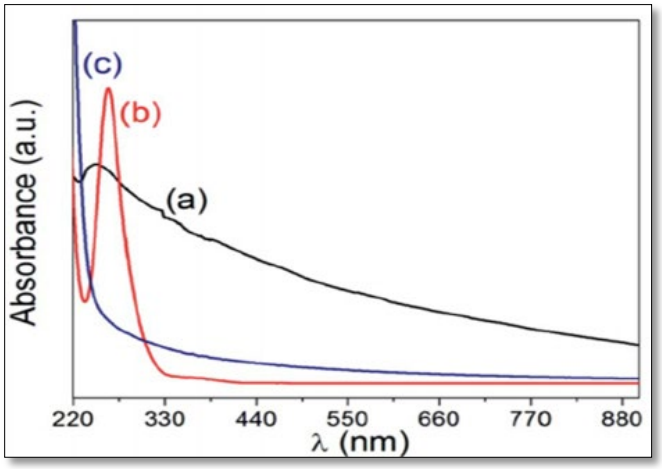

Figure 6. The UV-Vis spectra of GO–Chm nancomposite (b) after samples dispersed in water with sonication and 24 h kept to rest: (a) Chitosan; (b) GO–Chm nancomposite; (c) Graphine oxide.

X-ray diffraction patterns

Representative X-ray diffraction patterns of Fe_3O_4 and GO–Chm nancomposite is illustrates in **Figures 7A-a and 7A-b**, respectively. XRD spectrum of shows seven diffraction peaks at 2θ=30.10°, 35.42°, 37.05°, 43.05°, 53.39°, 56.94° and 62.52° are detected, which matches well with the indexed peaks of GO–Chm nancomposite, are consistent with the standard XRD data for the crystalline planes of face-centered cubic (fcc) Fe_3O_4 according to the standard spectrum of Fe_3O_4 (JCPDS, No. 65-3107). This indicated the coexistence of Fe_3O_4, chitosan and GO in the hybrid. As shown in Figure 8B, the magnetic hysteresis loop of the Fe_3O_4-GO–Chm hybrid is measured at room temperature with an applied magnetic field sweeping from -5000 to +5000 Oe, exhibiting super paramagnetic property of the magnetic nanocomposite. **Figure 7B** shows the magnetization of GO–Chm nancomposite in the range of ± 20 kOe. It can be seen that the hysteresis loops of the GO–Chm nancomposite sample are essentially overlapped in both the S-shape and when passing through the origin. The saturated magnetization (Ms) of the sample is 42.14 emu/g, which is lower than that of the pure Fe_3O_4 (74.0 emu/g). This may be due to that the GO–Chm is composed of the non-magnetic GO–Ch and the magnetic Fe_3O_4. The insert on the right of **Figure 1B** shows that with an external magnetic field, the GO–Chm adsorption-treated sample was adsorbed on the "magnetized" wall of the reaction vessel in a short period of time. Indeed, GO–Chm exhibits super paramagnetism and meets the requirements of magnetic separation. The GO–Chm nancomposite shows high thermal stability, it was determined and confirmed by TG-DSC curves.

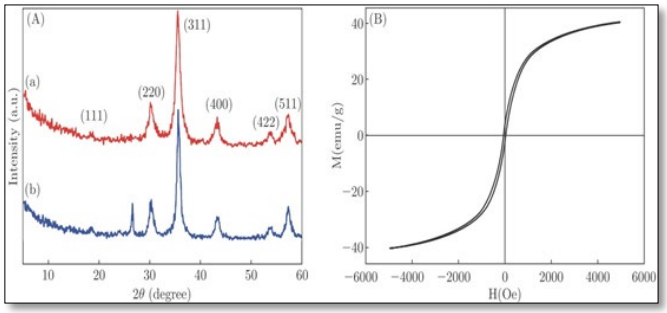

Figure 7. (A) X-ray diffraction patterns of (a) Fe_3O_4; and (b) GO–Chm nancomposite. (B) Magnetization hysteresis loop of GO–Chm nancomposite.

Thermogravimetric (TGA) measurements

Figure 8 shows thermogravimetric analysis (TGA) of magnetic chitosan, GO and GO–Chm nancomposite has been done at 20 μC/min heating rate under nitrogen. The thermal stability of the composite material has been assessed by TGA while keeping the material in an inert atmosphere. **Figure 8a** shows thermogravimetric analysis of GO, **Figure 9b** shows thermogravimetric analysis of Chm **Figure 8c** shows thermogravimetric analysis of GO–Chm nancomposite. The onset temperature for pure Chm degradation is about 350°C that is attributed to the main-chain pyrolysis. At 450°C, the total amount of polymer seemed to be pyrolyzed. It is found from **Figures 7c-7e** that the samples containing three GO–Chm nancomposites exhibited similar thermal stability. This may be explained by the following. The initial weight loss due to evaporation of solvent occurs at low temperature which is common to both

pure GO and GO–Chm. With the increase of temperature beyond 300°C, typically weight loss due to the change of mode (or phase) occurs in the sample. The identical thermal behavior of the pure GO and GO–Chm probably indicates that Chm remains inert in case of GO–Chm composite. These materials also exhibit similar thermal stability, and shows higher weight loss compared to others at the same temperature. The initial degradation observed between 200 and 280°C in these composites is caused by the elimination of the oxygen-containing groups in the oxidized graphene nanoplatelets during reaction with magnetic chitosan to form GO–Chm nancomposite. The second degradation observed between 350 and 480°C happens due to the degradation of the nanocomposite polymer itself. These results also suggest that there is a strong interaction between Chm and GO nanoplatelets at the interface, and the mobility of the polymer chains near the interface is decreased because of this interaction.

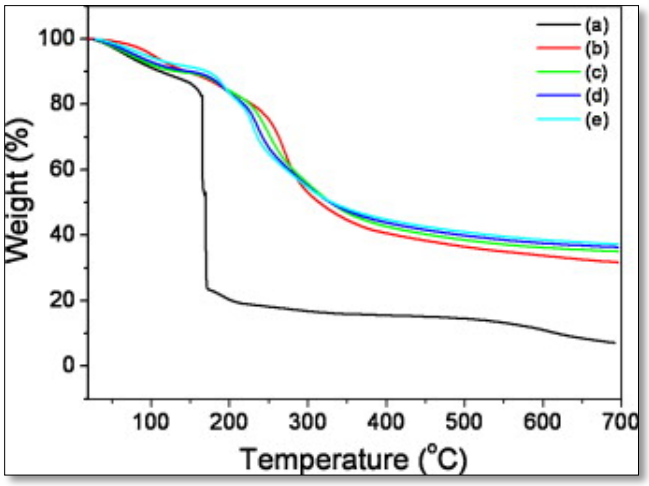

Figure 8. Thermogravimetric analysis (TGA) of (a) GO (b) chitosan (c, d, e) three samples of GO–Chm nancomposite.

Differential scanning calorimetry (DSC) measurements

Differential Scanning Calorimetry (DSC) measurements confirm a strong interaction between magnetic chitosan and graphene with the nanostructures matrix. DSC thermograms shown in **Figure 9** are obtained for magnetic chitosan and graphine and GO–Chm nanocomposites. From these heat scans, one can see the integrated area of the melting transition of the samples, containing magnetic chitosan copolymer-modified GO nanocomposite. In this GO weight fraction, the relative crystallinity of the copolymer-modified GO–Chm sample has been increased by about 5%, compared to the one of neat matrix. This crystallinity increase improve that the polymer chains were immobilized and reacted through hydrophobic and hydrogen bonding interactions with the GO. Thus, the order of relative crystallinity in our samples (at 1 wt% graphene loading) for copolymer-modified GO is found to be greater than the neat matrix. The fact that the sample of 3% wt GO exhibited a 15% decrease in crystallinity compared to neat magnetic chitosan could be attributed to the inhomogeneous in dispersion of GO aggregates into the matrix. The melting endothermic peak of neat matrix which was observed at about 230°C was slightly decreased in the composites. This result could be caused by the relatively smaller crystal size of Chm and due to the interaction of Chm into GO to form GO–Chm nanocomposite.

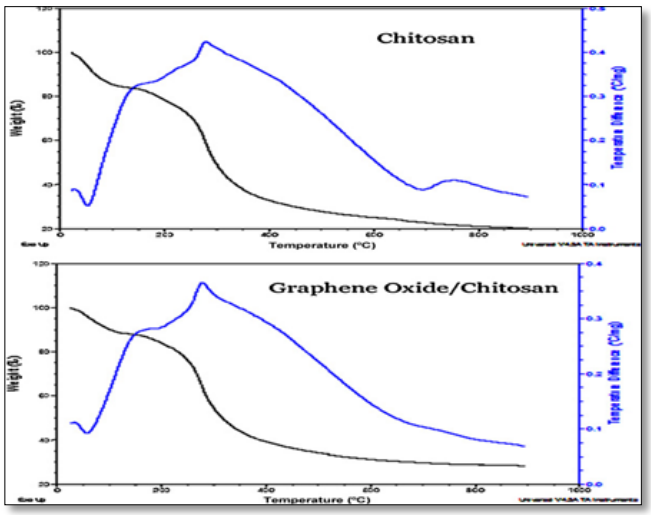

Figure 9. DSC thermograms of GO–Chm nancomposite.

Dielectric and conductivity properties of GE-CH

Figure 10a shows the electrical conductivity and the dielectric constants of the GO–Chm composites as a function of the volume fraction of the functionalized GO measured at 1 kHz and at room temperature. The electrical conductivity of the composite is observed to increase by more than five orders of magnitude with increase in GO concentration. The conductivity of GO–Chm nanocomposites increases near the percolation threshold which is found to be 3.5 vol%. Beyond the threshold, it exhibits a typical insulator-conductor transition. Conductivity of GO–Chm composites below the percolation threshold increases slowly with increasing GO volume fraction. The reason for this can be attributed to the tunneling conduction mechanism and percolation phenomenon between GO and Chm. The carboxylic groups on GO surface can reduce the tunneling current. **Figure 10b** shows the change in dielectric constant of GO–Chm composite as a function of the volume fraction of GO. As seen in the figure, the dielectric constant increases rapidly when the volume fraction of GO increases from 4 to 8 vol%. Then, the dielectric constant is found to decrease with increase in GE concentration. The maximum value of dielectric constant of the GO–Chm nanocomposites is observed to be 3200 which is obtained at 8 vol% of GO at 1 kHz frequency. Dielectric properties were measured using

an LCR meter (Agilent, E4980A) equipped with a dielectric test fixture (Agilent, 16451B) at the frequency 20 Hz to 2 MHz and at room temperature. Pure GO and its GO–Chm powders were pressed in the form of a disc pellet with a diameter of 25 mm by applying a pressure of 50 MPa in a hydraulic presser and the average thickness of the pellet was about 1.0 mm.

The dielectric properties of the nanocomposite have been explained by the percolation theory and interfacial polarization effect. In these composites, GO is distributed in the insulting matrix, which can form a lot of interfaces. When the concentration of GO increases, the number of interfaces also increases. This increases the dielectric constant with increasing GO concentration. When the concentration of GO is made larger than the percolation threshold of the composite, it results in agglomeration of GO. In this case, the interface between GO and Chm will decrease, thus resulting in reduction in dielectric constant with further increase in GO concentration. Probably the orbital of the GO also creates large domains for nomadic electrons. These electrons can produce interfacial polarization effect. Moreover, the carboxylic groups present in functionalized GO are electron-withdrawing groups that will strengthen interfacial polarization. The large value of dielectric constant (3200 at 8 vol% of GO) observed for GO–Chm nanocomposite can be attributed to increasing number of interfaces formed by GO and Chm matrix.

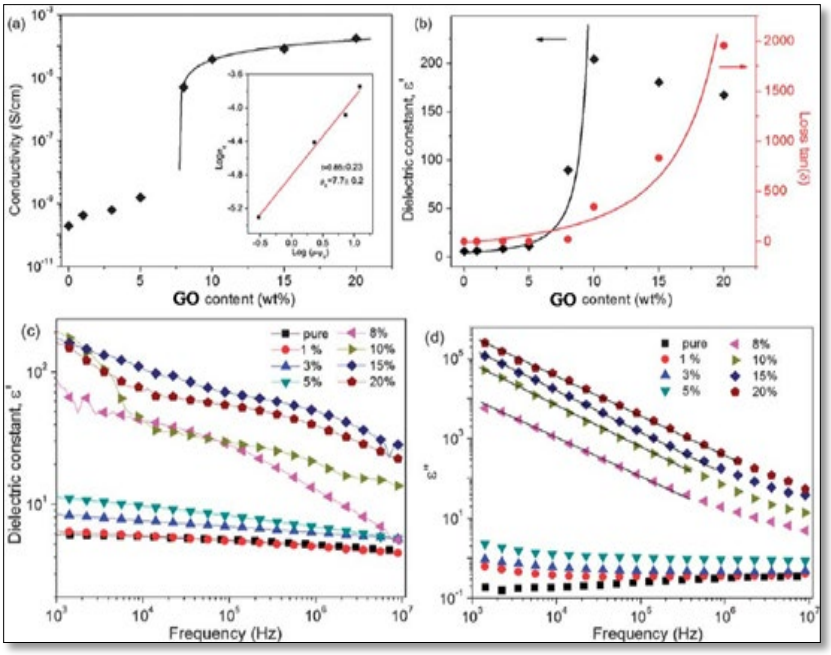

Figure 10. Dependence of the electrical conductivity and dielectric constant of GO nanocomposite on the volume fraction of GO (a) dielectric constant and dielectric loss tangent (b) of the GO–Chm composites at 1 kHz; frequency-dependent dielectric constant (c) and dielectric loss factor (d) of the GO–Chm composites as a function of the loading of GO s.

The drugs adsorption capacity

The drugs adsorption capacity was evaluated by placing the as-prepared GO–Chm nanocomposites in drugs aqueous solutions at pH 3. It should be noted that the adsorption process of freeze-dried samples seemed typical and easy to investigate. In the present work, the in situ adsorption behaviors of GO–Chm nanocomposites were chosen, which could demonstrate the real adsorption process of GO–Chm nanocomposites for different drugs in wastewater. In addition, GO–Chm has the probability to act as a visible light photocatalyst for degradation of drugs in the adsorption process. So the present adsorption experiments were measured and repeated in almost dark condition. The absorbance measurements were crried out at λ_{max}=356 nm for Tetracycline, λ_{max}=272 for Ciprofloxacin, λ_{max}=213.5 for ranitidine and λ_{max}=196 for lincomycin. In order to determine the concentration of drugs residual form wastewater samples, samples were collected at different time intervals. The drugs removal rates were calculated according to the equation of $K=(A_0 - A_T)/A_0 \times 100\%$, where K is the drug removal rate, A0 is the absorbance of the drug stock solution and AT is the absorbance of the supernatant liquid collected at different time intervals. **Tables 1 and 2** show the percent of drugs removal under visible and UV light, respectively. Under UV illumination tetracycline was almost completely degraded. The percent of drug removal using GO–Chm nanocomposites can reach nearly 100% for tetracycline under UV light and 90 under visible light. Tetracycline removal using GO reached 91% for tetracycline under UV light and 82 under visible light. Ciprofloxacin and ranitidine removal using GO–Chm nanocomposites 95% and

93% were removed under UV light 83% and 86% were removed under visible light, respectively. Ciprofloxacin and ranitidine removal using GO nanocomposites 90% and 86% were removed under UV light 82% and 80% were removed under visible light, respectively. Whereas for lincomycin both photocatalysts (GO and GO–Chm) showed similar performances. Nearly 89% for lincomycin under UV light and 72% under visible light were removed in the presence of GO–Chm. Nearly 81% for lincomycin under UV light and 69% under visible light were removed in the presence of GO nanocomposites. Thus, Graphene magnetic chitosan nanocomposites (GO–Chm) offer a green alternative to synthetic polymers in the preparation of soft nanomaterials for removal of drugs in wastewater.

Table 1. The compared remediation of drugs pollutants from wastewater with GO and GO–Chm nanocomposites in visible light.

Drug	Results[a] ± S.D. Using GO	Results[a] ± S.D. Using GO–Chm
Tetracycline	82	90
Ciprofloxacin	80	86
Ranitidine	82	83
Lincomycin	69	72

a: Mean of three determinations

Table 2. The compared remediation of drugs pollutants from wastewater with GO and GO–Chm nanocomposites in UV light.

Drug	Results[a] ± S.D. Using GO	Results[a] ± S.D. Using GO–Chm
Tetracycline	91	99.9
Ciprofloxacin	90	95
Ranitidine	86	93
Lincomycin	81	89

a: Mean of three determinations Effect of pH on drugs adsorption capacity

It should be mentioned that in the drugs adsorption capacity tests were investigated at pH values between 3 and 10 in the reaction solution. The results showed that when the pH value increase, the GO–Chm adsorption capacity toward drugs decreases gradually. The results show that an acidic environment is more favorable for the enrichment of drug on GO–Chm nanocomposite. This may be because the pH value of the solution affects the surface charge of the adsorbent and the form of drug in the solution. At low pH, the surface of GO–Chm is positively charged due to the protonation reaction. With increasing pH values, the surface of GO–Chm nanocomposite becomes negatively charged due to the deprotonation reaction. In addition, the pH value affects the ionization degree of the drugs molecules. For example, TC has three chemically distinct acidic functional groups: carboxymethyl (pKa=3.30), phenolic diketone (pKa=7.68) and dimethylamine cation (pKa=9.69). Thus, when the pH of the solution is less than 3.30, $H4TC^{+}$ ions are the dominant form of TC in the solution. When the pH is in the range of 3.30-7.68, TC can be thought of as a mixture of a dimethylamino group and a negatively charged hydroxyl group, with H3TC as the dominant form. When the pH is in the range of 7.68-9.69, $H2TC^{-}$ ions are the dominant form of TC. When the pH value of the solution is greater than 9.69, TC is mainly in the form of $HTC2^{-}$. At low pH, both GO–Chm and drugs are positively charged, while the highest sorption is observed, which may be due to that the covalent type/inner sphere type interactions are stronger than the non-specific electrostatic interactions of GO–Chm and drugs. In addition, the effects of ionic strength and humic acid on the removal of drugs by GO–Chm were investigated by using a series of drugs solutions containing different concentrations of NaCl (0-0.1 M). The result has shown that there are no significant differences on the adsorption capacity under the existence of these compounds. Therefore, this result further supports the fact that the adsorption process of drugs onto GO–Chm is inner sphere type. Although the Na^{+}, Cl^{-} and humic acid may interact with the TC molecular and the GO, the adsorption efficiency is almost independent of the ionic strength, indicating that the surface complexation of drug with GO–Chm is very strong.

At pH3 tetracycline and ranitidine drugs were adsorbed in the GO–Chm nanocomposite with maximum adsorption capacity of 575.5 mg/g and 218.2 mg/g, respectively. For ciprofloxacin and lincomycin the adsorption capacity at pH3 was 168 mg/g and 75 mg/g, respectively. Less than the adsorption capacity found in tetracycline and ranitidine. The most efficient adsorbent was the nanocomposite with 5 wt% GO, in acidic pH3 for all drug tested. It seems that acidic pH, enhance the adsorption process. The high surface area and abundant oxygen-containing functional groups of GO–Chm mean more available sites for binding drugs. Furthermore, surface complexation takes place between GO–Chm and drug due to hydrogen bonding or ion interactions with drug as well as π-π interactions of graphene with aromatic rings of drugs, because GO can act as a Lewis base due to its delocalized π-π electron system.

CONCLUSION

Based on our results, GO–Chm nanocomposite can be used for accumulation and removal of drugs from wastewater. The results show that an acidic environment is more favorable for the enrichment a degradation of drugs on GO–Chm nanocomposite. The pH value affects the protonation of the surface groups of the adsorbent, resulting in a change in surface charges available and affecting the chemical form

of drugs in the solution; these factors finally result in a decrease in the adsorption of drugs by GO–Chm with increasing pH. The drugs can form inner-sphere complexes with the surfaces of GO–Chm. The adsorption kinetics studies show that the kinetics data conform to the pseudo-second-order kinetics model. The maximum adsorption capacity for tetracycline and ranitidine were 575.5 mg/g and 218.2 mg/g, respectively. For ciprofloxacin and lincomycin the maximum adsorption capacity were 168.2 mg/g and 75.8 mg/g, respectively. High adsorption capacities were observed even after 4 cycles of adsorption tests, indicating that it has an excellent regeneration performance. The adsorption ability is based on hydrogen bonding or ion interactions with drug as well as π-π interactions of graphene with aromatic rings of drugs. Finally, the major conclusion of this work is the existence of a huge amount of literature regarding these types of polysaccharide/graphene-based nanocomposites and the opportunity existing to further expand graphene chemistry in order to synthesize more stable and effective materials with improved properties for innovative applications.

CONFLICTS OF INTEREST

The authors declare no conflict of interest regarding the publication of this paper.

REFERENCES

1. Passananti M, Lavorgna M, Iesce MR, Della Greca M, Brigante M, et al. (2015) Photochemical fate and eco-genotoxicity assessment of the drug etodolac. Sci Total Environ 518: 258-265.
2. Huang B, Liu Y, Li B, Liu S, Zeng G, et al. (2017) Effect of Cu(II) ions on the enhancement of tetracycline adsorption by Fe_3O_4@SiO_2-Chitosan/grapheme oxide nanocomposite. Carbohydr Polym 157: 576-585.
3. Yang Y, Hu X, Zhao Y, Cui L, Huang Z, et al. (2017) Decontamination of tetracycline by thiourea-dioxide-reduced magnetic graphene oxide: Effects of pH, ionic strength and humic acid concentration. J Colloid Interface Sci 495: 68-77.
4. Song W, Yang T, Wang X, Sun Y, Ai Y, et al. (2016) Experimental and theoretical evidence for competitive interactions of tetracycline and sulfamethazine with reduced graphene oxides. Environ Sci Nano 3: 1318-1326.
5. Kummerer K (2009) Antibiotics in the aquatic environment - A review-part. I. Chemosphere 75: 417-434.
6. Jung C, Son A, Her N, Zoh KD, Cho J, et al. (2015) Removal of endocrine disrupting compounds, pharmaceuticals and personal care products in water using carbon nanotubes: A review. J Ind Eng Chem 27: 1-11.
7. Yu F, Li Y, Han S, Ma J (2016) Adsorptive removal of antibiotics from aqueous solution using carbon materials. Chemosphere 153: 365-385.
8. Rattanachueskul N, Saning A, Kaowphong S, Chumha N, Chuenchom L, et al. (2017) Magnetic carbon composites with a hierarchical structure for adsorption of tetracycline, prepared from sugarcane bagasse via hydrothermal carbonization coupled with simple heat treatment process. Bioresour Technol 226: 164-172.
9. Kummerer K (2009) Antibiotics in the aquatic environment - A review-part II. Chemosphere 75: 435-441.
10. Kummerer K (2009) Antibiotics in the aquatic environment - A review-part I. Chemosphere 75: 17-434.
11. Baquero F, Martinez JL, Canton R (2008) Antibiotics and antibiotic resistance in water environments. Curr Opin Biotechnol 19: 260-265.
12. Wang D (2014) Pharmaceutical and personal care products in the surface water of China: A review. Chin Sci Bull (Chinese Version) 59: 743-748.
13. Arslan-Alaton I, Dogruel S (2004) Pre-treatment of penicillin formulation effluent by advanced oxidation processes. J Hazard Mater 112: 105-113.
14. Chelliapan S, Wilby T, Sallis PJ (2006) Performance of an up-flow anaerobic stage reactor (UASR) in the treatment of pharmaceutical wastewater containing macrolide antibiotics. Water Res 40: 507-516.
15. Chen WR, Huang CH (2010) Adsorption and transformation of tetracycline antibiotics with aluminum oxide. Chemosphere 79: 779-785.
16. Choi KJ, Son HJ, Kim SH (2007) Ionic treatment for removal of sulfonamide and tetracycline classes of antibiotic. Sci Total Environ 387: 247-256.
17. Koyuncu I, Arikan OA, Wiesner MR, Rice C (2008) Removal of hormones and antibiotics by nanofiltration membranes. J Membrane Sci 309: 94-101.
18. Ordikhani F, Tamjid E, Simchi A (2014) Characterization and antibacterial performance of electrodeposited chitosan-vancomycin composite coatings for prevention of implant-associated infections. Mater Sci Eng C Mater Bio Appl 41: 240-248.
19. Han D, Yan L, Chen W, Li W (2011) reparation of chitosan/graphene oxide composite film with enhanced mechanical strength in the wet state. Carbohydr Polym 83: 653-658.
20. Wang X, Bai H, Yao Z, Liu A, Shi G (2010) Electrically conductive and mechanically strong

biomimetic chitosan/reduced graphene oxide composite films. J Mater Chem 20: 9032-9036.

21. Yin H, Ma Q, Zhou Y, Ai S, Zhu L, et al. (2010) Electrochemical behavior and voltammetric determination of 4-aminophenol based on graphene-chitosan composite film modified glassy carbon electrode. Electrochimica Acta 55: 7102-7108.
22. He L, Wang H, Xia G, Sun J, Song R, et al. (2014) Chitosan/graphene oxide nanocomposite films with enhanced interfacial interaction and their electrochemical applications. Appl Surf Sci 314: 510-515.
23. Mohammadi MR, Mohammadi F, Mohammadi D, Fray J, Khomamizadeh F, et al. (2011) Template-based growth of titanium dioxide nanorods by a particulate sol-electrophoretic deposition process. Particuology 9: 161-169.
24. Fang M, Long J, Zhao W, Wang L and Chen G, et al. (2010) pH-responsive chitosan-mediated graphene dispersions. Langmuir 26: 16771-16774.
25. Wan Y, Lin Z, Zhang D, Wang Y, Hou B, et al. (2011) Impedimetric immunosensor doped with reduced graphene sheets fabricated by controllable electrodeposition for the non-labelled detection of bacteria. Biosens Bioelectron 26: 1959-1964.
26. Pati MK, Pattojoshi P, Roy GS (2015) Fabrication and characterization of graphene based nanocomposite for electrical properties. Adv Mater Phys Chem 5: 22-30.
27. Devi R, Relhan S, Pundir CS (2013) Construction of a chitosan/polyaniline/graphene oxide nanoparticles/polypyrrole/Au electrode for amperometric determination of urinary/plasma oxalate. Sensors Actuators B Chem 186: 17-26.
28. Li X, Zhou H, Wu WM, Wei S, Xu Y, et al. (2015) Studies of heavy metal ion adsorption on chitosan/sulfydryl-functionalized graphene oxide composites. J Colloid Interface Sci 448: 389-397.
29. Layek RK, Samanta S, Nandi AK (2012) Graphene sulphonic acid/chitosan nano biocomposites with tunable mechanical and conductivity properties. Polymer 53: 2265-2273.
30. Jagiello J, Judek J, Zdrojek M, Aksienionek M, Lipinska L, et al. (2014) Production of graphene composite by direct graphite exfoliation with chitosan. Mater Chem Phys 148: 507-511.
31. Krishnan D, Kim F, Luo J, Cruz-Silva R, Cote LJ, et al. (2012) Energetic graphene oxide: Challenges and opportunities. Nano Today 7: 137-152.
32. Singh V, Joung D, Zhai L, Das S, Khondaker SI, et al. (2011) Graphene based materials: Past, present and future. Prog Mater Sci 56: 1178-1271.
33. Malafaya PB, Silva GA, Reis RL (2007) Natural-origin polymers as carriers and scaffolds for biomolecules and cell delivery in tissue engineering applications. Adv Drug Deliv Rev 59: 207-233.
34. Shelke NB, James R, Laurencin CT, Kumbar SG (2014) Polysaccharide biomaterials for drug delivery and regenerative engineering. Polym Adv Technol 25: 448-460.
35. Kyzas GZ, Deliyanni EA, Matis KA (2014) Graphene oxide and its application as an adsorbent for wastewater treatment. J Chem Technol Biotechnol 89: 196-205.
36. Travlou NA, Kyzas GZ, Lazaridis NK, Deliyanni EA (2013) Graphite oxide/chitosan composite for reactive dye removal. Chem Eng J 217: 256-265.
37. Travlou NA, Kyzas GZ, Lazaridis NK, Deliyanni EA (2013) Functionalization of graphite oxide with magnetic chitosan for the preparation of a nanocomposite dye adsorbent. Langmuir 29: 1657-1668.
38. Kyzas GZ, Travlou NA, Deliyanni EA (2014) The role of chitosan as nanofiller of graphite oxide for the removal of toxic mercury ions. Colloids Surf B Biointerfaces 113: 467-476.
39. Kyzas GZ, Bikiaris DN, Seredych M, Bandosz TJ, Deliyanni EA, et al. (2014) Removal of dorzolamide from biomedical wastewaters with adsorption onto graphite oxide/poly (acrylic acid) grafted chitosan nanocomposite. Bioresour Technol 152: 399-406.
40. Du J, Cheng HM (2012) The fabrication, properties and uses of graphene/polymer composites. Macromol Chem Phys 213: 1060-1077.
41. Das TK, Prusty S (2013) Graphene-based polymer composites and their applications. Polym Plast Technol Eng 52: 319-331.
42. Sun X, Sun H, Li H, Peng H (2013) Developing polymer composite materials: Carbon nanotubes or grapheme. Adv Mater Weinh Ger 25: 5153-5176.
43. Kim H, Abdala AA, MacOsko CW (2010) Graphene/polymer nanocomposites. Macromolecules 43: 6515-6530.
44. Huang X, Qi X, Boey F, Zhang H (2012) Graphene-based composites. Chem Soc Rev 41: 666-686.
45. Zhang X, Rajaraman BRS, Liu H, Ramakrishna S (2014) Graphene's potential in materials science and engineering. RSC Adv 4: 28987-29011.

46. Tjong SC (2014) Polymer composites with graphene nanofillers: Electrical properties and applications. J Nanosci Nanotechnol 14: 1154-1168.

47. Kuang D, Hu WB (2013) Research progress of graphene composites. Wuji Cailiao Xuebao. J Inorg Mater 28: 235-246.

48. Rinaudo M (2008) Main properties and current applications of some polysaccharides as biomaterials. Polym Int 57: 397-430.

49. Draget KI, Skjåk-Bræk G, Smidsrød O (1997) Alginate based new materials. Int J Biol Macromol 21: 47-55.